Electronic Supplementary Material (ESI) for Journal of Analytical Atomic Spectrometry.

Electronic Supporting Information

Bayesian optimization of the conditions for highly sensitive detection of surface contamination by laser-induced breakdown spectroscopy

Tadatake Sato, Kenichi Tashiro, Yoshizo Kawaguchi, Hideki Ohmura, Haruhisa Akiyama

National Institute of Advanced Industrial Science and Technology (AIST), 1-1-1 Umezono, Tsukuba, Ibaraki 305-3568, Japan

Evaluation of surface concentrations

Samples coated with thin silicone oil layer was prepared by spraying system described in ref. 9. The amount of adhered silicone oil was evaluated from peak intensity of the IR band at 1266 cm^{-1} based on the linear relationship between peak intensity and surface concentration shown in Fig. S1 and Table S1. The amount of adhered silicone oil was weighed using a electric balance (Mettler Toredo Co., AG285).

Table S1. Weight of adhered silicone oil and IR peak intensity

Weight of adhered silicone oil (mg)	Calculated surface concentration (μg cm^{-2})	Peak intensity of IR band at 1266 cm^{-1}
0.134	7.42	0.213
0.208	11.52	0.276
0.268	14.84	0.430
0.278	15.39	0.444
0.152	8.42	0.237
0.172	9.52	0.295
0.308	17.05	0.433
0.344	19.04	0.509
0.148	8.19	0.225
0.220	12.18	0.320
0.288	15.94	0.425
0.316	17.49	0.487
0.116	6.43	0.180
0.162	8.97	0.241
0.226	12.51	0.359
0.312	17.27	0.473

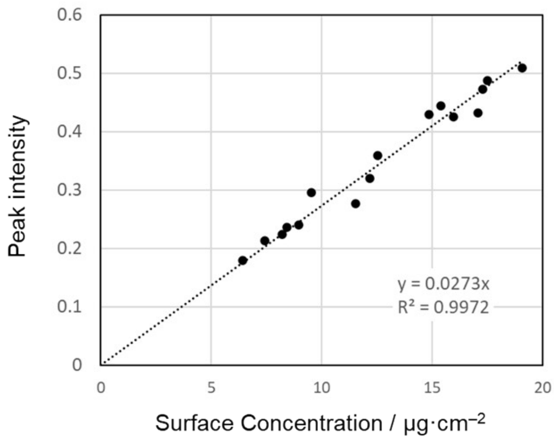

Fig. S1. Linear relationship between the IR band peak intensity at 1266 cm^{-1} and the surface concentration calculated from weight of adhered silicone oil.

Spot size and fluences

Spot size at various sZ was estimated from the etched structures formed by irradiation at 8.0mJ with 30 pulses. The generated structures were evaluated by laser confocal microscope (Keyence, VK-X1000). The long and short diameters of etched part are summarized in Table S2.

Table S2. Estimated spot size and fluences.

sZ	long diameter / μm	short diameter / μm	Area / cm^2	Fluence / J cm^{-2}							
				PE=8mJ	PE=7mJ	PE=6mJ	PE=5mJ	PE=4mJ	PE=3mJ	PE=2mJ	PE=1mJ
6.50	478.7	331.9	0.0012478	6.41	5.61	4.81	4.01	3.21	2.40	1.60	0.80
7.00	426.1	309.7	0.0010364	7.72	6.75	5.79	4.82	3.86	2.89	1.93	0.96
7.50	376.0	244.1	0.0007209	11.10	9.71	8.32	6.94	5.55	4.16	2.77	1.39
8.00	326.3	210.7	0.0005400	14.81	12.96	11.11	9.26	7.41	5.56	3.70	1.85
8.50	286.6	193.2	0.0004348	18.40	16.10	13.80	11.50	9.20	6.90	4.60	2.30
8.75	253.1	179.9	0.0003575	22.37	19.58	16.78	13.98	11.19	8.39	5.59	2.80
9.00	230.4	172.6	0.0003122	25.62	22.42	19.22	16.01	12.81	9.61	6.41	3.20
9.25	216.9	162.7	0.0002772	28.86	25.25	21.65	18.04	14.43	10.82	7.22	3.61
9.50	206.8	131.1	0.0002130	37.55	32.86	28.16	23.47	18.78	14.08	9.39	4.69
9.75	179.1	127.8	0.0001798	44.50	38.93	33.37	27.81	22.25	16.69	11.12	5.56
10.00	161.0	131.5	0.0001663	48.11	42.10	36.09	30.07	24.06	18.04	12.03	6.01
10.25	143.6	130.9	0.0001477	54.17	47.40	40.63	33.86	27.09	20.31	13.54	6.77
10.50	144.4	133.5	0.0001514	52.83	46.23	39.62	33.02	26.41	19.81	13.21	6.60
10.75	173.3	139.4	0.0001897	42.17	36.90	31.63	26.36	21.09	15.81	10.54	5.27
11.00	192.8	141.9	0.0002150	37.22	32.56	27.91	23.26	18.61	13.96	9.30	4.65
11.50	213.8	164.8	0.0002768	28.91	25.29	21.68	18.07	14.45	10.84	7.23	3.61
12.00	253.0	195.6	0.0003886	20.58	18.01	15.44	12.87	10.29	7.72	5.15	2.57
12.50	278.5	241.4	0.0005280	15.15	13.26	11.36	9.47	7.58	5.68	3.79	1.89
13.00	340.4	278.3	0.0007439	10.75	9.41	8.07	6.72	5.38	4.03	2.69	1.34
13.50	401.0	319.3	0.0010056	7.96	6.96	5.97	4.97	3.98	2.98	1.99	0.99
14.00	434.7	362.2	0.0012366	6.47	5.66	4.85	4.04	3.23	2.43	1.62	0.81

Details of Bayesian optimization process

The initial 40 conditions generated by Latin hyper cube sampling and the conditions employed in subsequent rounds are listed in Table S3. The numbers in parentheses denote the number of repeated experiments. These conditions were generated by a GPR model trained using the experimental results. In each round, the trained model was examined by plotting the correlation between the actual experimental results (r-LOD values) and the values predicted by the model. The results are summarized in Fig. S2 and the optimized kernel hyperparameters.

Table S3. Grid indices of experimental conditions until 10th round. The numbers in parentheses are the numbers of experiments

1st round				2nd	3rd	4th	5th	6th	7th	8th	9th	10th
85	602	1117	1564	120(2)	770	1327	185	402	140	121	61	52
120	619	1149	1575	119	769	384	16	582	122	130	787	70
280	642	1163	1671	129	590	761	392	131	132	113	121(2)	62
297	766	1193	1683	128	778	950	391	393	149	112	122(3)	79
315	767	1325	1752	111	581	291	92	573	131(2)	122(2)	131(3)	61(2)
396	820	1341	1867									
401	828	1382	1886									
458	957	1388	1911									
486	959	1512	1915									
498	978	1530	2074									

	Training at the 1st round; preparation for 2nd round	Training at the 2nd round; preparation for 3rd round	Training at the 3rd round; preparation for 4th round
	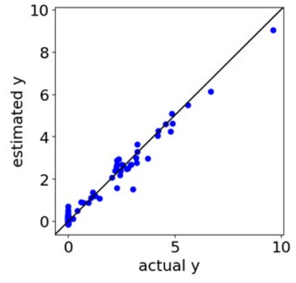	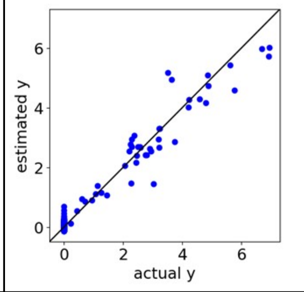	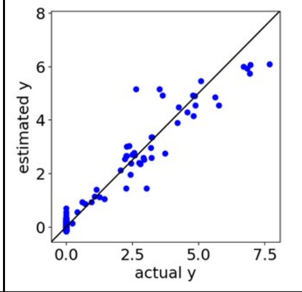
Setting of noise level bounds (upper and lower bounds)	(0.1, 0.5)	(0.1, 0.5)	(0.1, 0.5)
Log-Marginal-Likelihood	-185.749	-198.892	-210.752
R^2 fro the trained data	0.97769	0.96006	0.95100
length scale	0.714	0.709	0.7
noise level	0.1	0.1	0.1

	Training at the 4th round; preparation for 5th round	Training at the 5th round; preparation for 6th round	Training at the 6th round; preparation for 7th round
	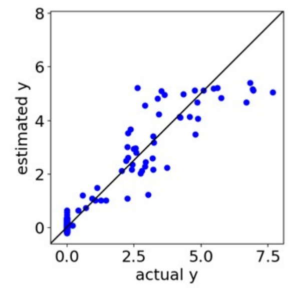	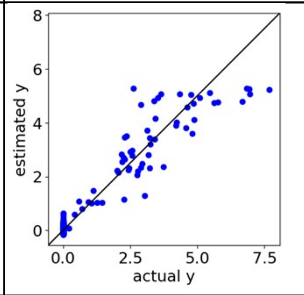	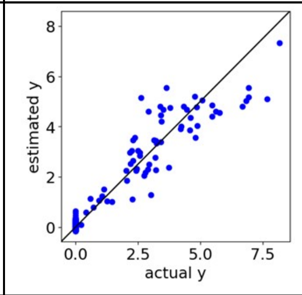
Setting of noise level bounds (upper and lower bounds)	(0.1, 0.5)	(0.02, 0.5)	(0.02, 0.5)
Log-Marginal-Likelihood	-234.082	-235.653	-228.600
R^2 fro the trained data	0.91395	0.92122	0.92473
length scale	0.875	0.805	0.841
noise level	0.103	0.0965	0.0919

	Training at the 7th round; preparation for 8th round	Training at the 8th round; preparation for 9th round	Training at the 9th round; preparation for 10th round
	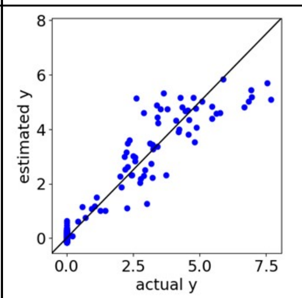	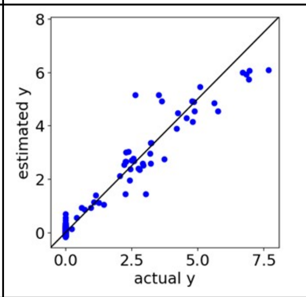	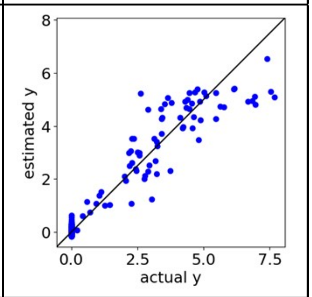
Setting of noise level bounds (upper and lower bounds)	(0.02, 0.5)	(0.02, 0.5)	(0.02, 0.5)
Log-Marginal-Likelihood	-218.904	-213.270	-206.169
R^2 fro the trained data	0.92546	0.92337	0.93033
length scale	0.831	0.863	0.853
noise level	0.0903	0.0913	0.0842

Fig. S2. The correlation between the actual r-LOD values and those predicted by the GPR model and optimized kernel hyperparameters at each round of Bayesian optimization.

The experimental conditions with PE of 7.0 and 7.5 mJ employed until the 10th round are shown in Table S4. In these conditions, the conditions with sZ around 8.25 or 12.75 mm and dZ = -0.5 − +0.5 mm were not included. The largest r-LOD was 5.622 obtained with grid index of 401.

Table S4. The conditions with PE = 7.0 and 7.5mJ examined until the 10th round

Grid index	PE (mJ)	sZ (mm)	dZ (mm)	r-LOD ($cm^2 \cdot \mu g^{-1}$)	No. of exp. (Round of exp.)
185	7.5	5.75	0.5	2.017	1(5)
280	7.5	11.25	-1.5	4.580	1(1)
291	7.5	11.75	-0.5	3.390	1(4)
297	7.5	12.25	-2.0	2.503	1(1)
315	7.5	13.25	-2.0	2.942	1(1)
384	7.0	6.75	1.0	5.465	1(4)
391	7.0	7.25	0.0	2.176	1(5)
392	7.0	7.25	0.5	4.611	1(5)
393	7.0	7.25	1.0	3.789	1(6)
396	7.0	7.75	-2.0	2.450	1(1)
401	7.0	7.75	0.5	5.622	1(1)
402	7.0	7.75	1.0	5.461	1(6)
458	7.0	10.75	2.0	1.059	1(1)
486	7.0	12.75	-2.0	2.206	1(1)
498	7.0	13.25	-0.5	3.242	1(1)

Selection of 13 conditions for 11th round

The conditions for the 11th round were manually selected based on the following criteria: (1) the conditions that showed the top 10 largest r-LODs in one experiment (grid indices:770, 111, 581, 959, 787, and 128), and (2) the conditions near these conditions showing low r-LOD. Three conditions with grid indices of 761, 591, and 950 were selected as shown in Fig. S3, where the distance $|\mathbf{x}_i - \mathbf{x}_j|$ is evaluated using autoscaled values. (3) the conditions with PE of 7.0 and 7.5 mJ with sZ around 8.25 or 12.75 mm and dZ = +0.5 mm: four conditions listed in Table S5 were selected. Thus, 13 conditions were selected for the experiments in the 11th round.

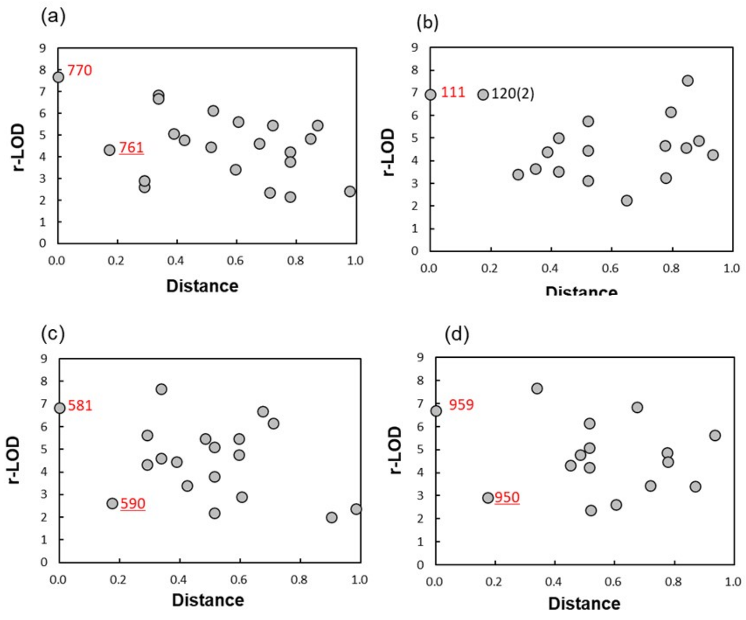

Fig. S3. r-LOD vs. distance $|\mathbf{x}_i - \mathbf{x}_j|$ from the conditions with grid indices of (a) 770, (b) 111, (c) 581, and (d) 959.

Table S5. Four conditions with PE of 7.0 and 7.5mJ for 11th round of experiment

Grid index	PE (mJ)	sZ (mm)	dZ (mm)
302	7.5	12.25	0.5
482	7.0	12.25	0.5
239	7.5	8.75	0.5
419	7.0	8.75	0.5

The grid indices of the conditions employed from 11th to 16th rounds are listed in Table S6. From the experimental results obtained in each round, the top 10 largest r-LOD values are listed in Table S7 together with the grid indices of the conditions. From the experiments in the 11th round, three conditions with 959, 787, and 128 disappeared from the table, whereas the r-LOD values of three conditions were corrected as follows:7.678 to 6.592 (grid index:770), 6.929 to 6.506 (grid index:111), 6.841 to 5.233 (grid index: 581). The conditions for the 12th round were generated using the GPR model, which was trained by adding the experimental results obtained from the 11th round.

Table S6. Grid indices of experimental conditions employed at the 11th ~ 16th round. The number in parentheses are that of repeated experiments. The numbers in bold stye indicates the manually selected conditions.

11th		12th	13th	14th	15th	16th
302	**787(2)**	1527	130(3)	112(2)	113(2)	614
482	**950(2)**	222	139	411	778(2)	1131
239	**959(2)**	121(3)	967	120(3)	140(2)	441
419		130(2)	**401(2)**	**402(2)**	**419(2)**	840
111(2)		131(4)	**384(2)**	**61(3)**	**770(3)**	140(3)
128(2)						
581(2)						
590(2)						
761(2)						
770(2)						

TableS7. Top 10 conditions showing the largest r-LOD at the 10th ~ 16th round

Round10		Round11		Round12		Round13	
Grid index	r-LOD	Grid index	r-LOD	Grid index	r-LOD	Grid index	r-LOD
770	7.678	131(3)	7.542	61(2)	7.019	61(2)	7.019
131(3)	7.542	61(2)	7.019	120(2)	6.929	120(2)	6.929
61(2)	7.019	120(2)	6.929	131(4)	6.617	131(4)	6.617
111	6.944	770(2)	6.592	770(2)	6.592	770(2)	6.592
120(2)	6.929	111(2)	6.506	111(2)	6.506	111(2)	6.506
581	6.841	122(3)	6.159	122(3)	6.159	122(3)	6.159
959	6.685	401	5.622	401	5.622	402	5.461
122(3)	6.159	384	5.465	384	5.465	401(2)	5.375
787	6.147	402	5.461	402	5.461	121(3)	5.333
128	5.761	581(2)	5.233	121(3)	5.333	581(2)	5.233

Round14		Round15		Round16	
Grid index	r-LOD	Grid index	r-LOD	Grid index	r-LOD
131(4)	6.617	131(4)	6.617	131(4)	6.617
770(2)	6.592	111(2)	6.506	111(2)	6.506
111(2)	6.506	120(3)	6.440	120(3)	6.440
120(3)	6.440	61(3)	6.302	61(3)	6.302
61(3)	6.302	122(3)	6.159	122(3)	6.159
122(3)	6.159	140(2)	5.814	401(2)	5.375
401(2)	5.375	401(2)	5.375	121(3)	5.333
121(3)	5.333	121(3)	5.333	770(3)	5.254
581(2)	5.233	770(3)	5.254	581(2)	5.233
419	5.202	581(2)	5.233	402(2)	5.172

The GPR model trained using the results of the 12th round yielded the five conditions as follows: grid indices of 130(2), 121(3), 139(0), 967(0), and 131(4), for the 13th round. The numbers in parentheses denotes the number of experiments conducted until the 12th round. Although multiple experiments are effective in correcting the variation, the conditions showing the top 10 largest r-LOD in the 12th round still include three conditions (grid indices:401, 384, and 402) under which only one experiment had been performed. Therefore, among the conditions given by the GPR model, those with grid indices of 121 and 131, experiments had been performed three and four times, respectively, were replaced by those with the grid indices of 401 and 384. For the 14th round, the conditions with grid indices of 402 and 61 were selected from those showing the top 10 largest r-LODs, in addition to the three conditions given by the GPR model (grid indices of 121, 130, and 131). For the 15th round, conditions with grid indices of 419 and 770 were selected, in addition to the three conditions given by the GPR model. After the 15th round of experiments, all conditions showing the top 10 largest LODs were the results of multiple experiments. Among these, two results from the 15th round were included (grid indices of 140 and 770). Moreover, by adding the results at the 15th round, the GPR model showed significant changes in hyperparameters and correlation between the actual and predicted values (Fig. S4). Therefore, successive round of experiments were executed. Whereas the five conditions employed in the 15th round were those for multiple experiments, the five conditions for the 16th round given by the GPR model included four conditions for the first experiment. In the 16th round, r-LOD values greater than 5.109 were not obtained. Therefore, the top 10 conditions with the largest r-LOD did not include the experimental results obtained in the 16th round. Thus, we terminated the optimization in this round.

	Training at the 11th round; preparation for 12th round	Training at the 12th round; preparation for 13th round	Training at the 13th round; preparation for 14th round
	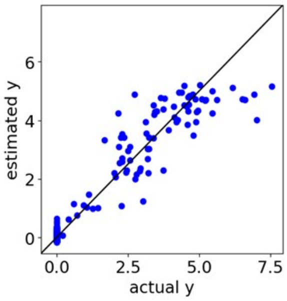	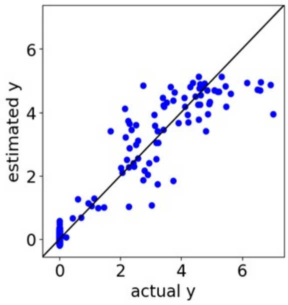	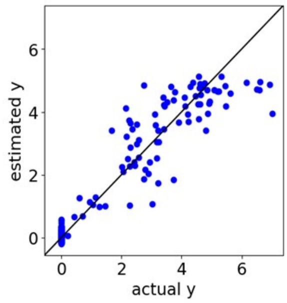
Setting of noise level bounds (upper and lower bounds)	(0.02, 0.5)	(0.02 0.5)	(0.02, 0.5)
Log-Marginal-Likelihood	-203.641	-197.484	-197.021
R^2 fro the trained data	0.92895	0.92425	0.92647
length scale	0.850	0.950	0.903
noise level	0.0851	0.0881	0.0863

	Training at the 14th round; preparation for 15th round	Training at the 15th round; preparation for 16th round	
	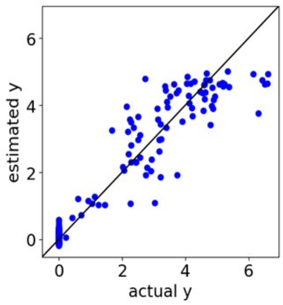	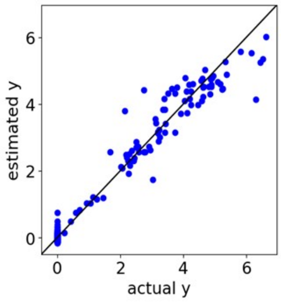	
Setting of noise level bounds (upper and lower bounds)	(0.02, 0.5)	(0.02, 0.5)	
Log-Marginal-Likelihood	-184.272	-171583	
R^2 fro the trained data	0.93172	0.97353	
length scale	0.891	0.544	
noise level	0.0806	0.0412	

Fig. S4. The correlation between the actual values and the values predicted by the trained model and the parameters at each round of Bayesian optimization (11th ~ 15th round).

Effect of air breakdown

The lowest LOD was obtained for LIBS measurements below the focal point. Generally, LIBS measurements with irradiation below the focal point are avoided to eliminate the effect of air breakdown. The luminescence of air breakdown was observed upon laser irradiation without samples at the focal point with a PE of 6.0−8.0 mJ. However, the luminescence of the air breakdown was much dimmer than the light emission in the LIBS measurements, and could not be detected by the present system. This was due to low PE. Chen et al. reported the threshold energy for detecting emission is 11 mJ for the fundamental pulse of an Nd:YAG laser (Y. -L. Chen, et. al., *J. Quant. Spectrosc. Radiat. Transf.*, 2000, **67**, 91–103.). The emission spectra of air breakdown showing peaks of N at 742.36, 744.23, and 746.83 nm, and those of O at 777.19, 777.42, and 777.54 nm were obtained with double-pulse bursts with a total pulse energy of 230 mJ (V. Sturm and R. Noll, *Appl. Opt.*, 2003, **42**, 6221–6225.). Fig. S5 shows that the LIBS spectra obtained above and below the focal point are almost identical. Although O and N peaks were detected, their intensities under the two conditions were similar. Therefore, they were derived from the atomic species excited in the plasma of the ablated substrate and not from air breakdown. Thus, the direct effect of air breakdown was not observed in the spectra. Considering that the PE of the conditions above and below the focal points were different, different spatial distributions of the laser light may cause different plasma heating. Further investigation is necessary to confirm this hypothesis.

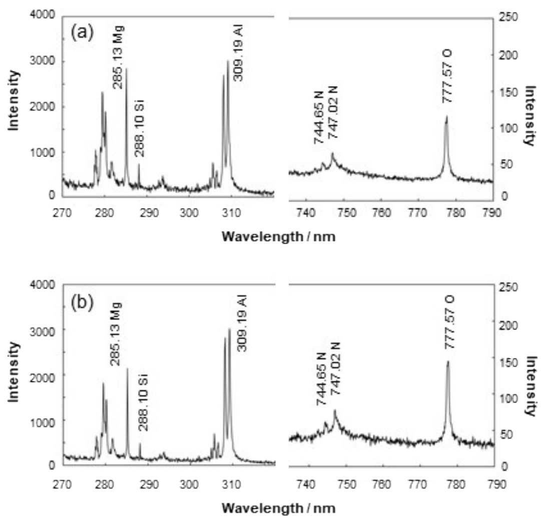

Fig. S5. LIBS spectra obtained under the conditions (a) above and (b) below the focal points.